

# Fully integrated holographic-Bragg-reflector-based mux/demux devices

D. Iazikov<sup>1</sup>, C. Greiner, and T. W. Mossberg

*LightSmyth Technologies, Inc., 860 W. Park, Suite 250, Eugene, OR 97401*

## ABSTRACT

A dual-channel, integrated, multiplexer, based on holographic Bragg reflector (HBR) devices and exhibiting flat-top, 4-nm-wide channels is demonstrated. Theory calibrated by the achieved performance indicates that HBR waveguide grating devices can be implemented to provide fully integrated and high performance multiplexer solutions for CWDM and FTTH applications. The enabling HBR devices can be regarded as mode-specific photonic crystals, i. e. photonic crystals whose spatial structure is tailored to interact with a specific signal mode or a very narrow range of such modes. Unlike standard bandgap-based photonic crystals, mode-specific photonic crystals may be effectively implemented with low-refractive-index-contrast and hence low-loss materials.

**Index terms:** apodization, flat-top filter, coarse WDM, FTTH, holographic Bragg reflectors, planar hologram, planar lightwave circuits, mode-specific photonic crystal.

## 1. INTRODUCTION

The development of inexpensive yet robust and high-performance optical multiplexing filters for datacom, coarse WDM (CWDM) and fiber-to-the-home (FTTH) applications poses an exciting challenge and opportunity to the optical community. We recently reported on a promising building-block element for distributed photonic circuits, which we refer to as a Holographic Bragg Reflector (HBR)<sup>[1], [2]</sup>. HBRs combine the best features of thin film filters (TFFs), fiber Bragg gratings (FBGs)<sup>[3]-[5]</sup>, as well as monolithically integrated devices such as arrayed-waveguide gratings (AWGs)<sup>[6]</sup> and lattice-form filters while avoiding many of their limitations. FBGs and TFFs offer powerful, potentially channel-specific, passband control, but typically lead to assembled systems of daisy-chained discrete filters. Package size and fabrication complexity of such assembled systems increases drastically with the number of channels involved. Furthermore, the footprint of assembled packages is limited by the approximately 2" minimum bending diameter required for long-term mechanical reliability of standard telecom interconnection fiber. Compact four channel CWDM with stacked TFFs were recently reported<sup>[7]</sup> and avoid such limitations at the expense of higher insertion loss and lower isolation. Monolithically integrated multiplexers have attracted wide attention due to their compactness and batch-fabrication potential fuelling numerous advances in planar lightwave circuit (PLC) fabrication<sup>[8]</sup>. AWGs are integrated and well-suited to provide large numbers of identical channels, but passband tailoring is limited and efforts to flatten the AWG passband result in an increase in insertion loss of several dB, therefore making such devices not a preferable choice for designing flat-top wideband filters. Lattice-form-filter-based four channel CWDM with good isolation and tractable insertion loss has been demonstrated<sup>[9]</sup>. However, such filters require multi-stage Mach-Zender interferometers (16 stages were used in<sup>[9]</sup>), and the complexity, size and fabrication sensitivity of the filters increase drastically with the number of the multiplexed channels. In contrast, HBR multiplexing technology is indeed both integrated, easily scales with the number of channels and provides passband control potentially as powerful as or superior to that of FBGs and TFFs. Flat-top wideband HBR-based filters may still have close to 100% passband reflectivity in a very compact footprint and, therefore, are especially well-suited for CWDM and FTTH-type applications. An important advantage of HBRs is their full compatibility with straightforward mature PLC fabrication and packaging techniques, which in turn enables fast design-implementation turnaround.

Much attention has been directed recently to photonic crystal devices especially those involving photonic bandgaps. HBR devices involve a related structural ordering of dielectric materials, however, HBR-type order is signal-mode

---

<sup>1</sup> diazikov@lightsmyth.com

selective. Optical signals not matched to a particular HBR typically pass through it with little effect. We refer to HBR's alternatively as mode-specific photonic crystals. Unlike traditional photonic crystals whose function usually requires high refractive index contrast and hence large loss (especially in 2D geometries), mode-specific photonic crystals (HBR's) function through highly cooperative and potentially long-range scattering. As a result, they can be implemented with very low refractive index and hence low loss materials. On the other hand, if HBR's are implemented with high refractive index contrast materials, their sizes can be shrunk to the same tiny scale offered in traditional photonic crystal devices.

The CWDM-relevant HBR devices demonstrated here comprise two-channel multiplexing devices having flat-top, 4-nm-wide, channel passbands implemented on a  $1 \times 5 \times 32$  mm silica-on-silicon optical chip. Device simulations, incorporating the present results and easily achievable enhancements in HBR structure, indicate that HBR-based, CWDM multiplexers having 16 channels, 13-nm flat-top passbands, and 1 to 2 dB fiber-coupled insertion loss should ultimately be obtainable on a die 5 mm x 20 mm in size. Since the HBR format is consistent with low-cost stamping/embossing-based fabrication, HBR-type CWDM and FTTH components (e. g. triplexers) may ultimately be provided at uniquely low costs.

## 2. HBR MULTI-CHANNEL FILTERS/MULTIPLEXERS

A two-channel HBR is shown schematically in Figure 1. It comprises a computer-generated, 2D, distributed Bragg reflective structure with nano-scale features photolithographically-scribed on the upper core-cladding interface of a single-mode silica-on-silicon planar waveguide. We refer to the structure as a holographic Bragg reflector since it is comprised of etched diffractive contours that can in general be optimized in the manner of a computer-generated hologram (or aspheric optic) to effect virtually any desired spatial wavefront transformation required to map input signal wavefronts optimally onto device output ports. Successive diffractive contours are placed precisely so as to impart desired (generally constructive) phase delays between successive diffracted wavefronts. Additionally, despite the essentially binary nature of the photolithographic process employed, flexible control over the diffractive amplitude of each contour can be implemented by several means including the variation of the fraction of each contour actually scribed, i. e. diffractive contours are written as dashed lines with the dash percentage proportional to the desired diffractive amplitude<sup>[10]</sup>. With precise control over both diffractive amplitude and phase of each of the thousands of diffractive contours involved, one can program the reflection spectrum of the device to have very general properties. In particular, broad and very flat-top reflective bandpass functions difficult to achieve with AWGs can be engineered – without compromising throughput. Owing to the fabrication method employed (laser-written reticle plus DUV photolithography) precise amplitude and phase control down to the level of individual diffractive contours is straightforward – a situation to be contrasted with that pertaining to FBGs where depth of focus constraints prevent single-line scribing. Note that in Figure 1 light is transported to and from the slab waveguide region via channel

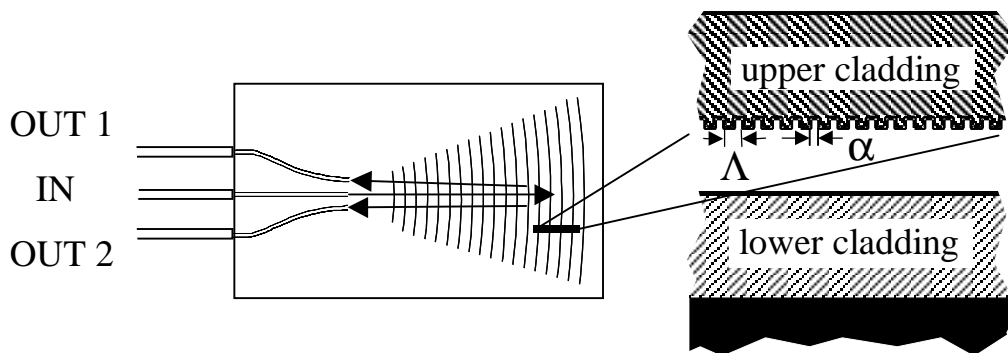


Figure 1. Left: Schematic top view of HBR. Right: Blow-up cross-sectional schematic of HBR.

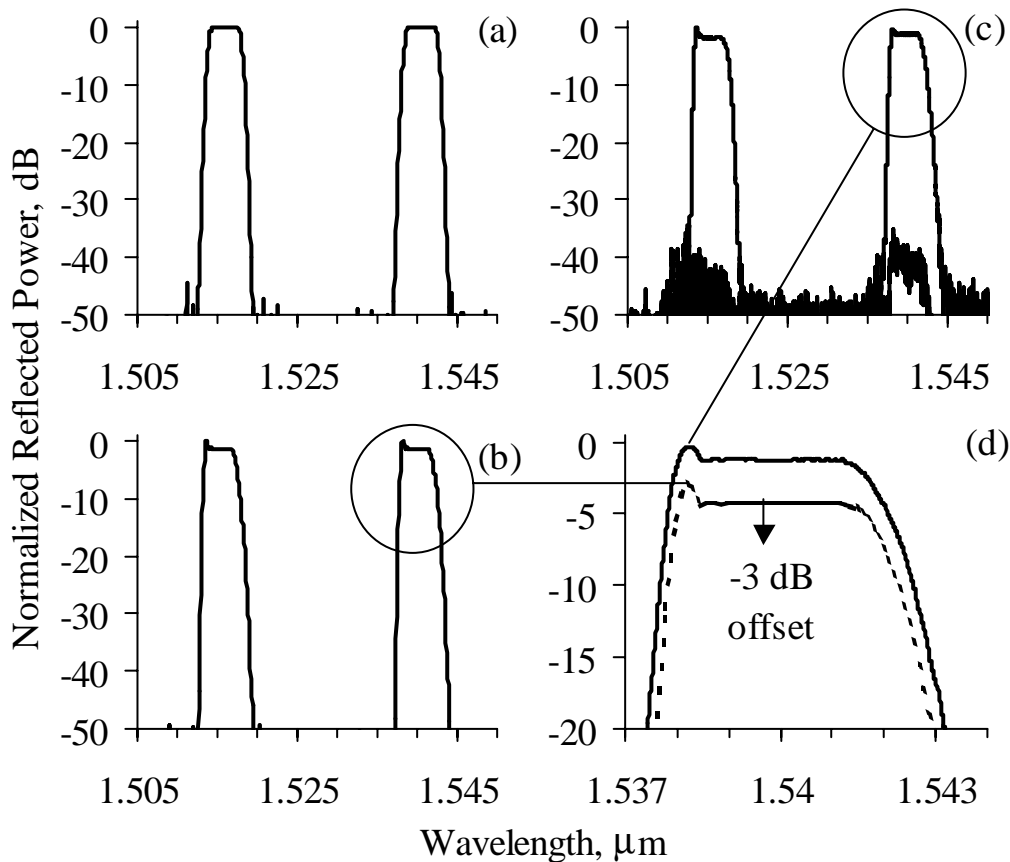


Figure 2. (a) Simulated relative device throughput versus wavelength with constant  $n_{\text{eff}}$ . (b) Simulated relative device throughput versus wavelength including variation of  $n_{\text{eff}}$  with amplitude apodization weight (c) Measured device throughput versus wavelength. (d) Blow-up comparison of left-most channel in (b) (dashed line) and (c) (solid line); for clarity of comparison, (b) is vertically offset by (-3 dB).

waveguides. Separate sets of diffractive contours image the input channel waveguide onto each of the output channel waveguides and provide for port-specific and independently programmable spectral transfer functions, hence multiplexing. HBR devices, with arbitrary contour design and powerful apodization pathways, contrast to the fixed non-apodized elliptical contoured slab waveguide filters demonstrated some years ago before flexible photolithographic means of 0.25 μm resolution were generally available<sup>[11]</sup>. Elliptical reflectors were discussed in the context of point-to-point imaging. More sophisticated imaging methods providing optimized overall wavefront mapping may be achieved via holographic imaging. The non-optimal nature of simple, conic-section, point-to-point imaging is well known in the optical design field.

### 3. DEVICE PERFORMANCE

The present device was fabricated using standard silica-on-silicon deposition, DUV-photolithography, and reactive-ion etching. The core and the cladding thicknesses are 2 μm and 15 μm, respectively. The core-cladding refractive index contrast is ~ 0.8% and the depth of the grating elements etched into the core is 400 nm. The width of the grating elements ( $\alpha$  in Fig. 1) was roughly 250 nm (50% duty cycle) and the pitch ( $\Lambda$  in Fig. 1) was about 0.5 μm consistent with first-order Bragg reflection for light in the vicinity of 1.5 μm (vacuum) wavelength. Diffractive element contours are circular lines imaging the common input port onto two distinctive output ports displaced by 60 μm on opposite sides

of the input port. Input and output ports comprise channel waveguides that are spaced by 250  $\mu\text{m}$  at the edge of the HBR die. The channel waveguides are adiabatically tapered in width from 12.7  $\mu\text{m}$  at the channel-slab waveguide interface to 6  $\mu\text{m}$  at the die edge. For testing, SMF28 optical fibers were butt-coupled to the channel waveguides at the die edge. The two displaced but partially overlapped HBRs employed in the multiplexer were pie-shaped, about 5 mm in width and 1.1 cm in length, with a lengthwise overlap of  $\sim 0.2$  cm.

Figures 2a, 2b, and 2c, respectively, show a simple simulation of expected device performance, a refined simulation of device performance incorporating apodization-induced variations in waveguide effective refractive index, and measured throughput of both channels of the fabricated HBR. The spectrum demonstrates very good channel isolation of  $\sim 40$  dB and steep roll-off. The measured insertion loss in the center of the passband is found to be 5 dB including a fiber-to-waveguide coupling loss of about 1 dB. The primary source of loss was low overall reflectivity which can be corrected with simple modification to HBR internal structure as discussed below.

The measurements shown employ polarized input signals. Polarization-dependent wavelength shifts of  $\sim 0.65$  nm were observed but do not interfere with the wide passbands of interest here or in CWDM generally. Measurements in similar devices having HBR's of differing diffractive orders reveal that polarization-dependent shifts arise from fabrication-related residual material birefringence rather than intrinsic HBR function<sup>[12]</sup>. No detectable polarization-dependent-insertion loss associated with reflectivity or scattering was observed. Recent observations of devices produced with a multi-layer core show an essentially complete elimination of polarization-dependent wavelength shifts.

It should be noted that for applications where multiplexer channels are separated by tens of nanometers and with multi-nanometer passbands (such as CWDM or a FTTH), silica-on-silicon HBR devices as described here can be considered essentially polarization and temperature insensitive. Specifically, the design flexibility inherent to the HBR approach allows one to design polarization and temperature insensitive devices by tailoring the multiplexer passband to have small ripple, steep roll-off, and incorporating guardbands to protect against polarization- and temperature-induced wavelength shifts. Assuming that the wavelength shift with temperature,  $\Delta\lambda$ , is caused primarily by the temperature dependence of the refractive index of silica ( $dn/dT = 1.1 \times 10^{-5} \text{ }^\circ\text{C}^{-1}$ <sup>[13]</sup>), the latter is estimated to be  $\Delta\lambda \sim \pm 0.4$  nm over the operating range of  $0^\circ\text{C}$  to  $70^\circ\text{C}$ . Consequently, both temperature- and polarization-dependent shifts represent only a small fraction of a typical CWDM channel bandwidth (13 nm), and hence can be protected against using tractable guardbands.

The HBR employed for each multiplexer channel is chirped to achieve the 4-nm spectral bandpass observed in Figure 2. If the HBRs were not chirped, their 1-cm length would produce an unsaturated 3-dB-linewidth of  $\approx 0.1$  nm. (Tests of unchirped HBRs reveal that the photolithographic methods employed do indeed provide transform-limited spectral response for cm-scale devices<sup>[12], [14]</sup>). In addition to the chirp in diffractive element spacing, each HBR was apodized in amplitude and phase to minimize passband ripple. The achieved passband profile (Fig 2c) closely duplicates the designed passband (Fig 2a) except for a narrow spike on the short wavelength side of the passband. We find that the spike results from a coupling of the effective-waveguide refractive index to the amplitude apodization approach employed, i. e. partial scribing of HBR contours. Measurements of separate test structures, confirmed by mode solver simulations, indicated that the effective refractive index of the slab waveguide,  $n_{eff}$ , can be approximated in the form

$$n_{eff} = n_o - 4.5 \times 10^{-4} G(r),$$

where  $G(r)$  is the fraction of each diffractive contour written at each position,  $r$ , within the device and  $n_o$  is the effective index of the slab waveguide in the absence the HBR contours. Simulations taking this effect into account produced the bandpass profiles of Figure 2b, which are in excellent agreement with the measured profile in Fig. 2c (see detailed comparison of Figure 2d). Compensating for amplitude-apodization-induced changes in effective waveguide refractive index is easily achieved in HBR design. Passband profiles in Figs. 2a and 2b are calculated using an explicit spatial model of the computer-generated HBR structure as it was submitted to the fabrication process. Calculations employed time-consuming but standard Fresnel diffraction methods. These are expected and found to be highly accurate in the weak reflection limit pertaining to the present devices. To design in the high reflectivity limit, the extensive set of tools developed in the context of apodized fiber Bragg gratings can be readily implemented<sup>[15], [16]</sup>.

#### 4. REFLECTIVE STRENGTH AND BANDWIDTH CONSIDERATIONS

HBR devices are reflective in nature. More specifically, they depend on cooperative reflection from distributed arrays of diffractive elements (contours) each of which is by itself a weak scatterer. There are fundamental constraints that connect the total number,  $N$ , of diffractive elements in an HBR (or alternatively the length,  $L$ , of the HBR), the diffractive scattering amplitude of each element,  $r_a$ , the total spectral bandwidth over which the device is to reflect,  $\Delta\nu$ , and the required reflective strength. Coarse WDM devices (e. g. a 16-channel multiplexer) require high reflectivity over an aggregate bandwidth that may be as large as several hundred nanometers. We wish to estimate the spectral bandwidth (which may or may not be contiguous) over which a first-order HBR of constrained length  $L$  and simple internal geometry can provide high reflectivity. Consider the quarter-wave reflective stack shown in Figure 3a<sup>[17]</sup>. The stack consists of planar interfaces between materials of refractive index  $n_1$  and  $n_2$ . Let  $\Delta n = |n_2 - n_1|$  and  $n = (n_1 + n_2)/2$ . The planar interfaces are spaced by  $\Lambda/2$  and produce strong Bragg backscattering at vacuum wavelength  $\lambda_B = 2n\Lambda$ .

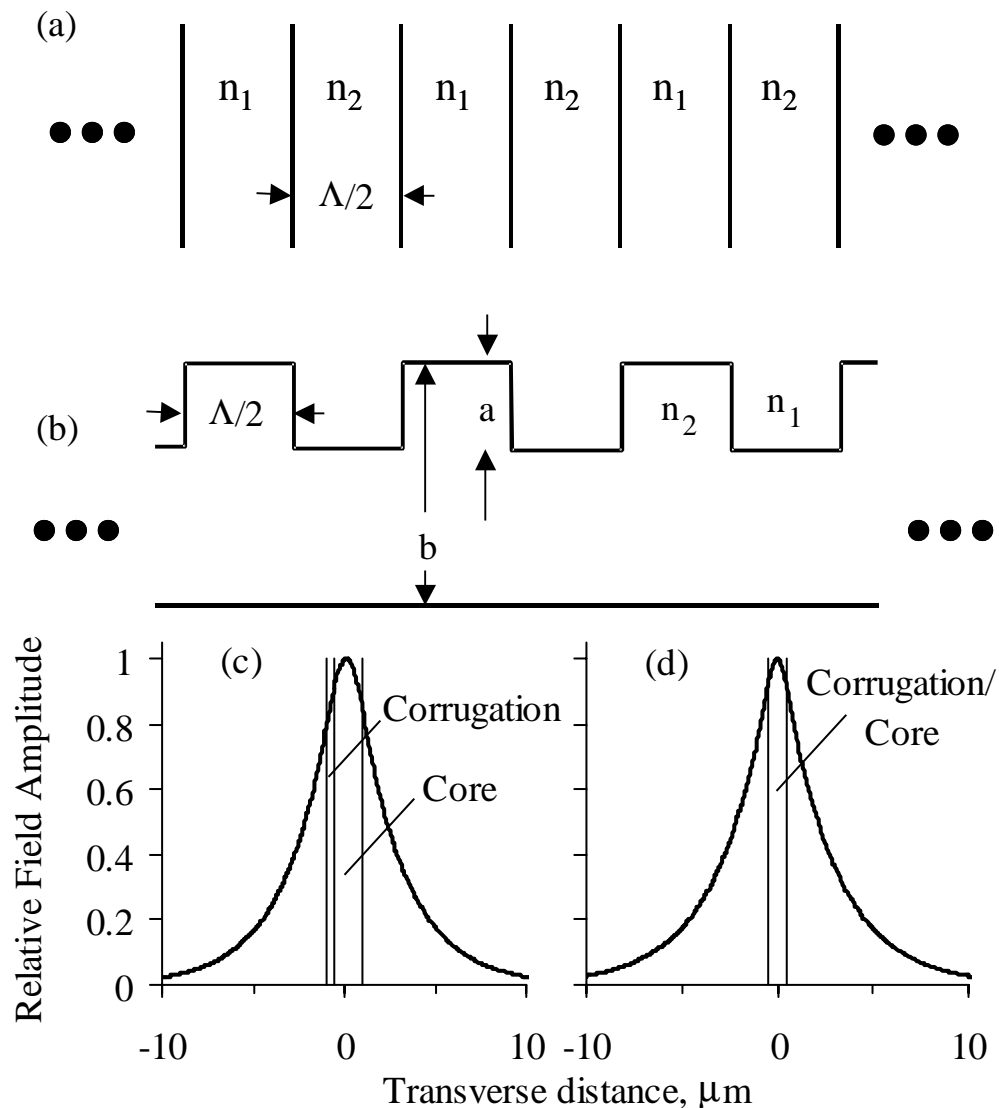


Figure 3. (a) Quarter-wave stack of planar interfacial reflectors. (b) Corrugated planar waveguide reflector model of HBR. (c) Plot of modal electric field for the corrugated slab waveguide configuration fabricated and tested ( $0.4 \mu\text{m}$  corrugation etched in  $2 \mu\text{m}$  thick waveguide). (d) Plot of the modal electric field for a very broad reflection bandpass slab waveguide structure (see text).

The incident wave (assumed incident normal to the interfaces) is attenuated and exhibits a 1/e penetration depth of approximately  $d = n\Lambda/q\Delta n$  [17], where factor  $q$  is defined as the ratio of back scattered field amplitudes produced by the corrugation and plane interfaces. For the quarter-wave stack,  $q = 1$ . The corrugated slab waveguide of Figure 3b exhibits similar behavior except that the factor  $q$  is less than one. A regular diffractive structure of length  $d$  has a weak-signal Fourier-transform spectral bandpass of approximately  $\Delta\nu_d \approx c/4nd$ , where  $c$  is the vacuum light speed. We use this bandwidth to approximate that of diffractive structures of 1/e field penetration. In the following, we assume that an HBR of length  $L > d$  may be viewed as a number of segments of length,  $d$ , each of which has bandwidth  $\Delta\nu_d$  and operates at 1/e field transmission. To achieve a broad reflection band, the various HBR segments are chirped or frequency shifted. The construction described is consistent with an overall HBR reflection bandwidth  $\Delta\nu_{tot}$  given by

$$\Delta\nu_{tot} = \frac{L}{d} \Delta\nu_d = \frac{cL\Delta n^2 q^2}{4\Lambda^2 n^3}$$

Figure 3c depicts the electric field mode of a corrugated slab waveguide modeled after our fabricated structure. Calculating the field area under the corrugated region and dividing by the total field area, we determine  $q \approx 0.06$ . With  $L = 1$  cm,  $\Lambda = 0.5$   $\mu\text{m}$ ,  $n \approx 1.45$ , we get  $\Delta\nu_{tot} \approx 4 \times 10^{11}$  Hz which corresponds to about a 3-nm reflective bandwidth at the operative wavelength. The present model suggests that the fabricated devices should operate somewhat in the low to moderate reflectivity regime since their bandwidth spanned more than 3 nm – which indeed they were found to do as indicated by their 4 dB reflectivity-limited insertion loss. We shift our attention to predicting how one might produce an HBR capable of reflecting over several hundred nm as needed for general CWDM mux applications. In Figure 3d, we show the modal electric field for a 1- $\mu\text{m}$ -thick slab waveguide whose corrugations extend entirely through the slab ( $a=b$  in Figure 3b). The value of  $\Delta n$  has been increased by a factor of three to approximately 0.03. The  $q$  factor is found to be 0.16. With these parameters, we find that  $\Delta\nu_{tot} \approx 3 \times 10^{13}$  Hz, which corresponds to about a 210-nm reflective bandwidth at the operative wavelength – broad enough to support 16 13-nm-wide CWDM channels. It should be noted the etch aspect ratio needed to produce the described broadband HBR device has been demonstrated as part of the LightSmyth development program. Note further that a wide range of HBR internal designs are possible providing even broader reflection bands and fully consistent with low loss at the fiber to die interface. It appears entirely possible to integrate much of the current functionality attributed to discrete thin-film filters into the fully integrated environment.

## 5. SUMMARY

Harnessing the ever more widely available DUV photolithographic fabrication capabilities developed for the electronics industry and planar device fabrication processes developed largely in the context of AWGs, we have demonstrated a powerful integrated approach to some filtering/multiplexing applications now handled exclusively or nearly so by discrete TFFs. We have further presented a simple model suggesting that very broadband and widely configurable filters will be possible. We note that in CWDM applications, silica-on-silicon planar waveguide HBR devices will not require temperature control. Also, polarization-dependent passband shifts produced by residual material birefringence are not a serious design issue. The HBR integrated photonic device approach promises, through ultimate stamping/embossing-based fabrication, to support a uniquely low cost approach to producing filtering devices for coarse WDM, access WDM, and even datacom.

## REFERENCES

1. T. W. Mossberg, "Planar holographic optical processing devices," *Opt. Lett.*, vol. 26, no. 7, pp. 414-416, Apr 2001.
2. T.W. Mossberg, "Lithographic holography in planar waveguides", *SPIE Holography Newsletter*, vol. 12, no. 2, pp. 1,8, Nov 2001.
3. T. Erdogan, "Fiber Grating Spectra", *J. Lightwave Technol.*, vol. 15, no. 8, pp. 1277-1294, Aug 1997.
4. C.R. Giles, "Lightwave application of fiber Bragg gratings", *J. Lightwave Technol.*, vol. 15, no. 8, pp. 1391-1404, Aug 1997.
5. V. Mizrahi, T. Erdogan, D.J. DiGiovanni, P.J. Lemaire, W.M. MacDonald, S.G. Kosinski, S. Cabot, J.E. Sipe, "Four channel fibre grating demultiplexer", *Electronics Letters*, vol. 30, iss. 10, pp. 780-781, May 1994.
6. M. K. Smith and C. van Dam, "PHASAR-based WDM-devices: principles, design and applications", *IEEE J. Select. Topics Quantum Electron.*, vol. 2, pp. 236-250, June 1996.
7. H. Sasaki and Y. Okabe, "CWDM multi/demultiplexer consisting of stacked dielectric interference filters and off-axis diffractive lenses", *IEEE Photon. Technol. Lett.*, vol. 15, no. 4, pp. 551-553, April 2003.

8. Y. Hibino, "Recent advances in high-density and large-scale AWG multi/demultiplexers with higher index-contrast silica-based PLCs", *IEEE J. Select. Topics Quantum Electron.*, vol. 8, no. 6, pp. 1090-1101, November 2002.
9. Y. Inoue, et al. "Low-crosstalk 4-channel coarse WDM filter using silica-based planar lightwave circuit", *Optical Fiber Communication Conference 2002*, pp. 75-76, 17-22 March 2002.
10. D. Iazikov, C. Greiner, and T. W. Mossberg, "Effective gray-scale in lithographically-scribed planar holographic Bragg reflectors", *Appl. Opt.*, to appear Jan 2004.
11. C. H. Henry, R. F. Kazarinov, Y. Shani, R. C. Kistler, V. Pol, and K. J. Orlowsky, "Four-channel wavelength division multiplexers and bandpass filters based on elliptical Bragg reflectors", *J. Lightwave Technol.*, vol. 8, no. 5, pp. 748-755, May 1990.
12. C. Greiner, D. Iazikov, and T. W. Mossberg, "Lithographically-fabricated planar holographic Bragg reflectors", *J. Lightwave Technol.*, accepted for publication.
13. K. Okamoto, *Fundamentals of optical waveguides*, San Diego: Academic Press, 2000.
14. C. Greiner, D. Iazikov, and T. W. Mossberg, "Lithographically scribed, focusing, planar holographic Bragg reflector with 17-GHz pass-band and 0.3 cm<sup>2</sup> footprint", *Optical Fiber Communication Conference*, postdeadline paper PD31, Atlanta, Ga, March 23-28, 2003.
15. R. Feced, M. N. Zervas, and M. A. Muriel, "An efficient inverse scattering algorithm for the design of nonuniform fiber Bragg gratings", *IEEE J. Quantum Electron.*, vol. 35, no. 8, pp. 1105-1115, Aug 1999.
16. J. Skaar, L. Wang, and T. Erdogan, "On the synthesis of fiber Bragg gratings by layer peeling", *IEEE J. Quantum Electron.*, vol. 37, no. 2, , pp. 165-173, Feb 2001.
17. A. Yariv, P. Yen, *Optical waves in crystals*, New York: John Wiley & Sons, 1983.

Copyright 2004. Society of Photo-Optical Instrumentation Engineers (SPIE). This paper was published in the Proceedings of SPIE, Vol. 5355-13, January 2004, pp. 96-102, and is made available as an electronic reprint with permission of SPIE. One print or copy may be made for personal use only. Systematic or multiple reproduction, distribution, duplication of any material in this paper for a fee or for commercial purposes or modification of the content of the paper are prohibited.